Journal of New Materials for Electrochemical Systems 14, 203-207 (2011)

Structure and Electrochemical Performance of $LiNi_{0.8}Co_{0.15}Al_{0.05}O_2$ Cathodes Before and After Treatment with $Co_3(PO_4)_2$ or $AlPO_4$ by *in situ* Chemical Method

Yu-Rim Bak[1], Youngmin Chung[1], Jeong-Hun Ju[1], Moon-Jin Hwang[2], Youngil Lee[1] and Kwang-Sun Ryu[1,*]

[1]Department of Chemistry, University of Ulsan, Ulsan 680-749, Korea
[2]Energy Harvest-Storage Research Center, University of Ulsan, Ulsan 680-749, Korea

Received: March 31, 2011, Accepted: May 26, 2011, Available online: June 03, 2011

Abstract: *$Co_3(PO_4)_2$ or $AlPO_4$ coating layers were formed on the surface of $LiNi_{0.8}Co_{0.15}Al_{0.05}O_2$ cathode material by in situ chemical method and calcination at 700°C to improve the electrochemical cyclability and structural stability during charge-discharge process of the cathode. The structure and electrochemical properties of the pristine $LiNi_{0.8}Co_{0.15}Al_{0.05}O_2$ cathode materials and the metal phosphate coated-cathode materials were investigated by X-ray powder diffraction, scanning electron microscopy, particle size analysis, Brunauer-Emmett-Teller method, cyclic voltammetry, and galvanostatic charge-discharge test. $Co_3(PO_4)_2$-$LiNi_{0.8}Co_{0.15}Al_{0.05}O_2$ and $AlPO_4$-$LiNi_{0.8}Co_{0.15}Al_{0.05}O_2$ cathode showed the improved reversibility compared with the pristine cathode material. It is attributed to the structural stability of metal phosphate coated $LiNi_{0.8}Co_{0.15}Al_{0.05}O_2$. In particular, $Co_3(PO_4)_2$-$LiNi_{0.8}Co_{0.15}Al_{0.05}O_2$ showed a more stable rate capability than the pristine $LiNi_{0.8}Co_{0.15}Al_{0.05}O_2$ and $AlPO_4$-$LiNi_{0.8}Co_{0.15}Al_{0.05}O_2$ at high C-rate.*

Keywords: Surface coating, Cathode, Electrode, Electrochemical properties, Lithium ion batteries

1. INTRODUCTION

Lithium-nickel-cobalt mixed oxides have attracted much research interest in the region of lithium ion battery due to their positive effects on electrochemical property and cost [1,2]. The nickel rich alloys, $LiNi_{0.8}Co_{0.2}O_2$, with high capacity and medium cost are a positive cathode material for lithium ion battery but there are still hurdles to overcome before application for market [3,4]. The nickel rich $LiNi_{0.8}Co_{0.2}O_2$ has rapid H_2O and CO_2 uptake in air. Consequently, the impurities such as LiOH and Li_2CO_3 are formed on the surface of $LiNi_{0.8}Co_{0.2}O_2$ particles [5-7]. The bonding of Ni-O becomes weaker by the oxidation of $Li_2CO_2^-$ adjoining to nickel oxides. LiOH exposed in $LiPF_6$ electrolyte can lead to acidic by-product (HF), which dissolves metal ions from cathode materials. These side reactions result in thermal instability and gas generation at high storage temperature (90°C) [8].

Various doping ions, such as Co^{3+}, Mg^{2+}, Ti^{4+}, Al^{3+}, and F^-, were introduced to $LiNi_{0.8}Co_{0.2}O_2$ structure in order to improve cathode performance [9-11]. Al-doping is believed to be considerably useful because of strong Al-O bonding and electrochemically inactive property of Al ions for Li insertion and desertion reactions [12]. $LiNi_{0.8}Co_{0.15}Al_{0.05}O_2$ has an improved thermal stability and electrochemical performance during Li insertion and desertion reactions but the problems observed in nickel rich alloys should be overcome [13].

In order to minimize the thermal instability of nickel rich alloys, metal oxide (TiO_2) and metal phosphate coating (Al, Ce, SrH, and Fe) have been used for surface coating [14-16]. The improved thermal stability of coated cathode materials is mainly attributed to the property of coating material. Among the metal phosphate coating materials, cathode materials coated with $AlPO_4$ exhibited the enhanced thermal stability and reversible capacity due to their structural stability caused by strong covalent P-O bonding in PO_4 anion with Al ion. $AlPO_4$ coating has contributed to the superior initial discharge capacity compared with that of uncoated cathode material. It has been confirmed that the very small amount of Li_3PO_4 is formed throughout the reaction between $AlPO_4$ and excess Li on the surface of cathode material during heat treatment at 700 ºC but $AlPO_4$ coating is not effective to reduce the side reactions of lithium impurities (LiOH and Li_2CO_3) on the cathode material and electrolyte. Meanwhile, it has been reported that $Co_3(PO_4)_2$ can minimize a side reactions with electrolyte by the reactions with lithium impurities. Cho et al. firstly introduced

*To whom correspondence should be addressed: Email: ryuks@ulsan.ac.kr
Phone: +82 52 2592763; Fax.: +82 52 2592348

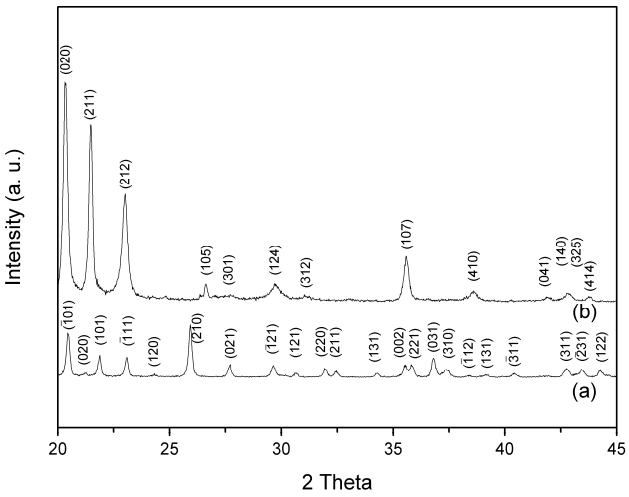

Figure 1. XRD patterns of (a) $Co_3(PO_4)_2$ and (b) $AlPO_4$.

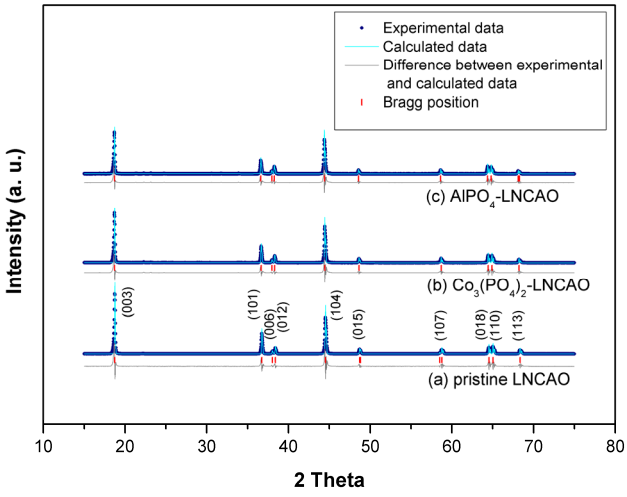

Figure 2. Rietveld refinement plots of (a) the pristine LNCAO, (b) $Co_3(PO_4)_2$-LNCAO, and (c) $AlPO_4$-LNCAO.

cobalt phosphate coating on $LiNi_{0.8}Co_{0.16}Al_{0.04}O_2$ [8]. They reported that the formation of an olivine Li_xCoPO_4 phase with below 20nm thickness on the surface of $LiNi_{0.8}Co_{0.16}Al_{0.04}O_2$ throughout the mixing of lithium-active $Co_3(PO_4)_2$ nanoparticles pre-synthesized and $LiNi_{0.8}Co_{0.16}Al_{0.04}O_2$ powders in aqueous solution, separation of coated powders, and consecutive calcination in air.

In this study, $Co_3(PO_4)_2$ coating was directly formed on the surface of pristine cathode materials using *in situ* chemical method compared with traditional coating method using mechanical mixing process. $Co_3(PO_4)_2$ nanoparticles prepared from the reaction of cobalt nitrate, $Co(NO_3)_2{\cdot}6H_2O$, and diammonium phosphate, $(NH_4)_2HPO_4$, were coated on the pristine materials in one step. Agglomeration of $Co_3(PO_4)_2$ nanoparticles on the surface of pristine materials gave rise to coating layer ranging several nanometer to submicrometer size during calcination. We expected that the increased reaction area of Li-active $Co_3(PO_4)_2$ coating layer by *in situ* chemical coating method would generate a positive effects on performance of Li ion batteries. The electrochemical performance of $Co_3(PO_4)_2$-$LiNi_{0.8}Co_{0.15}Al_{0.05}O_2$ was compared with that of the pristine and $AlPO_4$-$LiNi_{0.8}Co_{0.15}Al_{0.05}O_2$.

2. EXPERIMENTAL

2.1. Reagents and Synthesis

The $LiNi_{0.8}Co_{0.15}Al_{0.05}O_2$ (LNCAO) was used as a starting cathode material (Ecopro Co., Ltd., Korea). $Co(NO_3)_2{\cdot}6H_2O$, $(NH_4)_2HPO_4$, and $Al(NO_3)_3{\cdot}9H_2O$ were purchased from Sigma-Aldrich. In order to identify the formation of $Co(PO_4)_2$ and $AlPO_4$, 7.1g $Co(NO_3)_2{\cdot}6H_2O$ and 9.2g $Al(NO_3)_3{\cdot}9H_2O$ were dissolved in individual 50ml distilled water and 2~3g $(NH_4)_2HPO_4$ was added to the solution of metal nitrates to produce the precipitate. The precipitate was collected and heated at 700°C. The 3wt% $Co_3(PO_4)_2$ coating on the LNCAO, $Co_3(PO_4)_2$-LNCAO, was obtained by following process. 1.43g $Co(NO_3)_2{\cdot}6H_2O$ and 20g LNCAO were previously mixed in 10ml distilled water (DW). The 0.6g $(NH_4)_2HPO_4$ was added to cobalt nitrate solution and sonicated in an ultrasonic bath. After filtration of the precipitate with pink color, the precipitate was dried at 120°C, calcinated at 700°C, and naturally cooled to room temperature. The $AlPO_4$ (3wt%) coating on the pristine LNCAO, $AlPO_4$-LNCAO, was carried out by a similar method. The precipitate was produced by addition of the 0.65g $(NH_4)_2HPO_4$ into the mixture containing 1.85g $Al(NO_3)_3{\cdot}9H_2O$, 20g LNCAO, and 10ml distilled water. The precipitate was dried at 120°C and calcinated at 700°C.

2.2. Cell Assembly

The coin type half cells (2016R size) were prepared in an argon-filled glove box. The half cells were composed of a cathode, a Li metal anode, a microporous polyethylene separator, and an electrolyte solution. To prepare the cathode electrode 92wt% active material, 4wt% carbon black (super P), and 4wt% binder (PVDF) were used. The pristine LNCAO, $Co_3(PO_4)$-LNCAO and $AlPO_4$-LNCAO were used as active material for the cathode, respectively. 1.3M $LiPF_6$ dissolved in a 3:3:4 mixture of ethylene carbonate (EC), dimethyl carbonate (DMC), and ethylene methyl carbonate (EMC) by volume ratio was used as the electrolyte.

2.3. Physical and Electrochemical properties

The X-ray diffraction patterns were measured with a Rigaku ultra-X (CuKα radiation, 40kV, 120mA) at a step scan rate of 0.02°/sec in the 2θ range (10~70°) to identify the crystalline phase of the pristine LNCAO, $Co_3(PO_4)_2$-LNCAO, and $AlPO_4$-LNCAO. The morphologies and size of the samples were analyzed using scanning electron microscopy (SEM, Supra 40 - Carl Zeiss Co., Ltd.). The particle size and particle size distribution of the samples were examined by particle size analyzer (PSA, LS 13 320- BECK-MAN COULTER). The surface properties including specific surface area, BJH-pore volume, pore area, and pore diameter of the samples were characterized by BET analysis (BELSORP-II). Cyclic voltammetry(CV, Macpile biology) data of the cells were obtained at 2.8~4.8V and a 0.05mV sec^{-1} scan rate. The cells were galvanostatically charged and discharged with a current density of 0.05~3C in the range of 2.8~4.3V to determine the electrochemical behavior of the cathode materials.

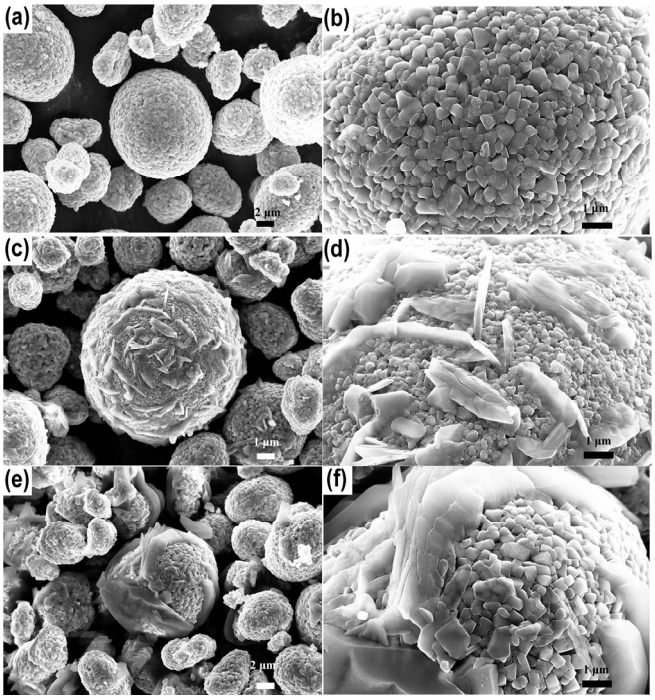

Figure 3. SEM images of (a, b) the pristine LNCAO, (c, d) $Co_3(PO_4)_2$-LNCAO, and (e, f) $AlPO_4$-LNCAO.

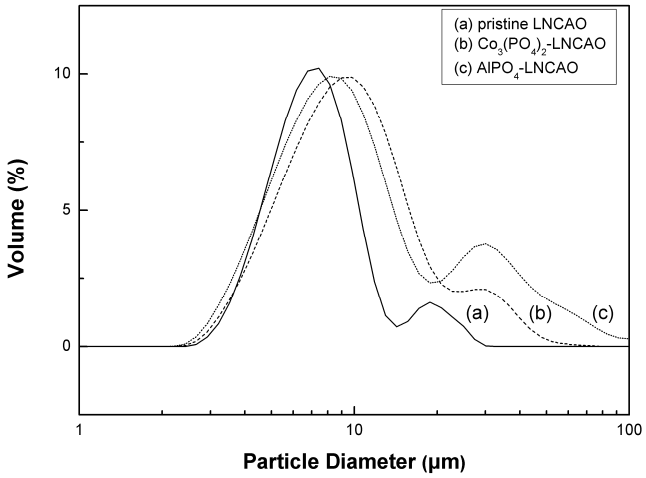

Figure 4. Particle size distributions of (a) the pristine LNCAO, (b) $Co_3(PO_4)_2$-LNCAO, and (c) $AlPO_4$-LNCAO.

3. RESULTS AND DISCUSSION

3.1. X-ray Powder Diffraction

The crystal phase of $Co_3(PO_4)_2$ and $AlPO_4$ as coating material was measured in the range of 2θ=20~45° in order to compare XRD patterns of the materials before and after coating. The $Co_3(PO_4)_2$ and $AlPO_4$ were obtained by the reaction of metal nitrate solutions and $(NH_4)_2HPO_4$ and calcination of the precipitate containing the metal ions at 700°C for 7hrs. XRD patterns are well matched with standard values (JCPDS card no.=48-0652) for $Co_3(PO_4)_2$ (Fig. 1(a)) and (JCPDS card no.=48-0652) for $AlPO_4$ (Fig. 1(b)).

Fig. 2 shows Rietveld refinement patterns of the pristine and the coated particles. The experimental diffraction peaks of the pristine and the coated particles indicate the formation of α-$NaFeO_2$ type layered structure belonging to a hexagonal-type $R\bar{3}m$ space group. The spectra also show clear split (006)/(012) and (018)/(110) peaks, indicating a well layered structure. The experimental diffraction peaks of $Co_3(PO_4)_2$-LNCAO and $AlPO_4$-LNCAO showed an identical peak patterns without showing any changes in site disordering. No impurity peaks of Li_2CO_3 and LiOH were observed from the diffraction patterns. However, the peaks assigned to $Co_3(PO_4)_2$ and $AlPO_4$ were not detected because the amount (~3wt%) of coating materials is relatively low compared with the pristine. Diffraction data was analyzed using Rietveld refinement programs (e.g. FullProf Suite Program, version 2007). Table 1 shows the lattice parameters and c/a value of the pristine LNCAO, $Co_3(PO_4)_2$-LNCAO, and $AlPO_4$-LNCAO. The hexagonal lattice parameters (a=2.8661 and c=14.1874) of the pristine LNCAO were varied with the effect of coating material. The lattice parameters (a and c) of the coated LNCAO increased than those of the pristine LNCAO. That indicates the formation of solid solution on the surface of LNCAO as well as the coating layer forming. The lattice parameters (a=2.8742 and c=14.2079) of $AlPO_4$-LNCAO were larger than those of $Co_3(PO_4)_2$-LNCAO (a=2.8706 and c=14.1995).

Table 1. Lattice parameters for the pristine LNCAO, $Co_3(PO_4)_2$-LNCAO, and $AlPO_4$-LNCAO.

	a (Å)	c (Å)	c/a	Unit cell volume (Å^3)
Pristine LNCAO	2.8661	14.1874	4.9501	100.93
$Co_3(PO_4)_2$-LNCAO	2.8706	14.1995	4.9465	101.33
$AlPO_4$-LNCAO	2.8742	14.2079	4.9432	101.65

3.2. Electron Microscopy

Fig. 3 shows scanning electron microscopy images of the pristine LNCAO and the coated samples after calcination at 700°C. The morphology of the pristine LNCAO shows a spherical bulk particles comprised of small particles less than 300nm (Fig. 3(a, b)). The formation of coating layer on LNCAO was clearly observed in Fig. 3(c-f). As shown in Fig. 3(c, d), LNCAO surface was irregularly covered by $Co_3(PO_4)_2$ particles with a slit-shaped structure with below 1 μm thickness. In Fig. 3(e, f), LNCAO particles were partially covered by $AlPO_4$ coating layers and the thickness of $AlPO_4$ coating was thicker than those of $Co_3(PO_4)_2$. The different shapes (Fig. 3(c-f)) of coating layer are believed to be dependent on the tendency of crystal growth of $Co_3(PO_4)_2$ and $AlPO_4$ during calcination.

3.3. Particle Size Analysis

Fig. 4 shows the particle size distribution of the samples. The particle size distribution of the coated sample shifted to larger particle size when compared with the pristine LNCAO (see Table 2).

The average particle size of the samples increased in order of the pristine LNCAO (8.48μm) < $Co_3(PO_4)_2$-LNCAO (12.28μm) < $AlPO_4$-LNCAO (17.13μm).

3.4. BET Analysis

The pore characteristics of the samples were obtained by the N_2 adsorption-desorption isotherms at 77K. The BET surface areas of the pristine LNCAO, $Co_3(PO_4)_2$-LNCAO, and $AlPO_4$-LNCAO were 0.37, 1.19, and 0.92$m^2 g^{-1}$, respectively. The low surface area of the pristine LNCAO means that the inner structure of the pristine LNCAO is dense. The increase of BET surface area observed in $Co_3(PO_4)_2$-LNCAO and $AlPO_4$-LNCAO is due to metal phosphates coating on LNCAO. The BJH mean pore diameter calculated from BJH desorption isotherms decreased in order of the pristine LNCAO (23.66nm), $AlPO_4$-LNCAO (8.31nm), and $Co_3(PO_4)_2$-LNCAO (5.13nm) (See Table 3). These results indicate that the spaces between small particles of LNCAO were covered by coating layer.

3.5. Cyclic Votammetry

The cyclic voltammograms for the pristine LNCAO, $Co_3(PO_4)$-LNCAO, and $AlPO_4$-LNCAO were taken at room temperature in the range 2.8~4.8V with a scan rate of 0.05mV s^{-1}. Fig. 5 shows the CV curves during 2~4 cycles after the first cycle. The location of anodic and cathodic peaks remained at the same position. Four anodic peaks (3.7, 3.9, 4.1, and 4.3V) and four cathodic peaks (3.5, 3.9, 4.1, and 4.4V) were observed in broad CV peaks of the pristine LNCAO, as shown in Fig. 5(a). The pristine LNCAO has a monoclinic phase (M) and a three hexagonal phases (H1, H2, and H3) such as $LiNiO_2$ [17]. Four peaks correspond to phase transformations of the pristine LNCAO to H1↔M↔H2↔H3. The CV curves of $AlPO_4$-LNCAO were similar to that of the pristine LNCAO but the areas of CV curves of $AlPO_4$-LNCAO were slightly decreased compared with the pristine LNCAO. The ΔV between the major anodic and cathodic peaks decreased from 0.27V of the pristine LNCAO to 0.21V of $AlPO_4$-LNCAO. The improved reversibility was observed in $AlPO_4$-LNCAO with the slight decrease of CV peaks. Three anodic/cathodic peaks, which are different from the pristine LNCAO and the $AlPO_4$-LNCAO, of $Co_3(PO_4)_2$-LNCAO were observed in Fig. 5(c). The CV peaks of $Co_3(PO_4)_2$-LNCAO show one pair of sharp anodic/cathodic peaks at 3.73/3.67V and

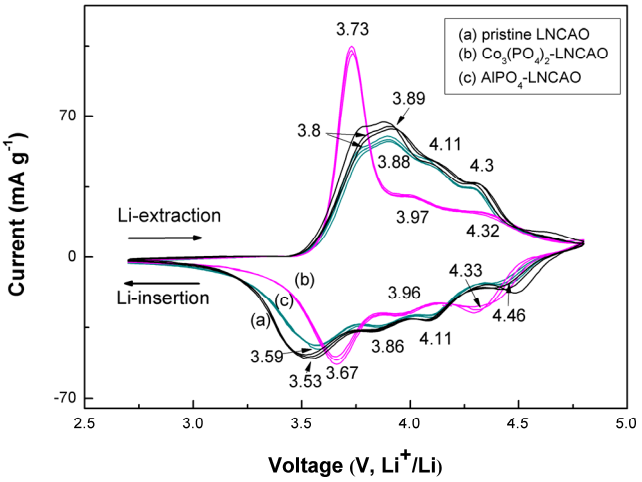

Figure 5. Cyclic voltammograms of (a) the pristine LNCAO, (b) $Co_3(PO_4)_2$-LNCAO, and (c) $AlPO_4$-LNCAO.

two pair of low and broad peaks located at about 4.0V and 4.3V. The relative low peaks at the range of 3.8 to 4.5V are originated from the suppression of phase transformation during charge-discharge reactions. In $Co_3(PO_4)_2$-LNCAO, the difference between the major anodic and cathodic peaks was reduced to 0.06V.

3.6. Charge-Discharge Profiles

Rate capability is one of the important electrochemical characteristics of a lithium secondary battery, and the improved rate capability is required for power storage applications. The charge/discharge process of the half cells was repeated five times for measuring the discharge capacity at 0.05, 0.1, 0.2, 0.5, 1, 2, and 3C in the range 2.8~4.3V. Fig. 6 shows the discharge capacity and cyclic property of the pristine LNCAO and the coated LNCAO cathodes. The initial discharge capacities of the pristine LNCAO, $AlPO_4$-LNCAO, and $Co_3(PO_4)_2$-LNCAO cells were 209, 208, and 197 mAh g^{-1}, respectively. $AlPO_4$ and $Co_3(PO_4)_2$ coating did not lead to any noticeable changes in discharge capacity profiles at 0.05~0.2C rate. The relatively low discharge capacity of $Co_3(PO_4)_2$-LNCAO may be due to the reduced rate of electron transfer caused by irregular distribution of $Co_3(PO_4)_2$ particles with a slit-shaped structure. As

Table 2. The particle size analysis of pristine LNCAO, $Co_3(PO_4)_2$-LNCAO, and $AlPO_4$-LNCAO.

	Pristine LNCAO	$Co_3(PO_4)_2$-LNCAO	$AlPO_4$-LNCAO
Mean(μm)	8.48	12.28	17.13
Median(μm)	7.46	9.99	10.00
Mean/Median	1.14	1.24	1.71
Mode(μm)	7.78	10.29	8.54
D_{10}(μm)	4.71	5.14	4.96
D_{50}(μm)	7.46	9.91	10.00
D_{90}(μm)	12.63	22.75	38.47

*Mean: average Median: middle grain size Mode: the most granularities
D_{90}, D_{50}, and D_{10} are the particle size when the percentage less than of the particle size distribution curve is 90, 50, and 10%, respectively.

Table 3. The BET analysis of the pristine LNCAO, $Co_3(PO_4)_2$-LNCAO, and $AlPO_4$-LNCAO.

	Pristine LNCAO	$Co_3(PO_4)_2$-LNCAO	$AlPO_4$-LNCAO
The specific BET surface area ($m^2 g^{-1}$)	0.3783	1.1987	0.9134
BJH total pore volume (V, $cm^3 g^{-1}$)	0.00304	0.00669	0.01256
BJH total pore area (A, $m^2 g^{-1}$)	0.129	1.300	1.511
BJH mean pore diameter (4V/A, nm)	23.66	5.13	8.31

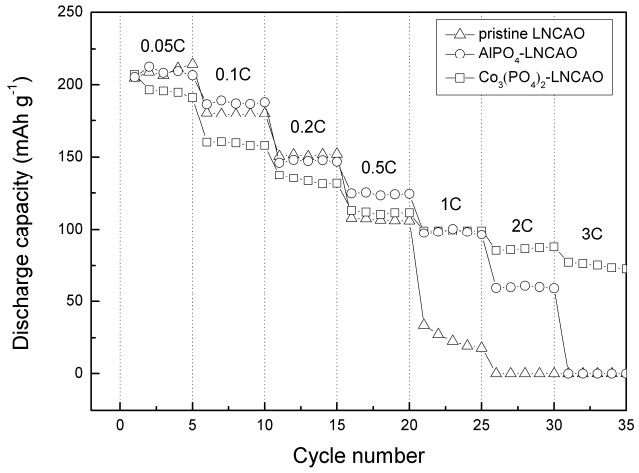

Figure 6. Cycling performances of the pristine LNCAO, $Co_3(PO_4)_2$-LNCAO, and $AlPO_4$-LNCAO at 2.8~4.3V.

the C-rate increased from 0.5 to 3C, the increased fading rate of discharge capacity was observed at the pristine LNCAO cell, while the relatively lower capacity fading was observed at the coated LNCAO. In particular, the $Co_3(PO_4)_2$-LNCAO cell showed a more stable rate capability than pristine LNCAO and $AlPO_4$-LNCAO. The better rate capability of the $Co_3(PO_4)_2$-LNCAO is consistent with the result from Fig. 5. It is estimated that lithium diffusivity within the cathode increased during charge-discharge cycles at high C-rate because of a stable surface structure of $Co_3(PO_4)_2$-LNCAO. A side reactions between lithium impurities and electrolyte could be minimized by lithium active $Co_3(PO_4)_2$ coating.

4. CONCLUSION

To improve the structural stability and rate capability of nickel rich $LiNi_{0.8}Co_{0.15}Al_{0.05}O_2$ (LNCAO) as cathode material, the $Co_3(PO_4)_2$ or $AlPO_4$ coating layer were formed on the surface of the pristine LNCAO by *in situ* chemical method. It was observed that the physical and the electrochemical properties of the coated material depend on the nature of coating material. At high C-rate, the better rate capability of the $Co_3(PO_4)_2$-LNCAO is attributed to its structural stability during lithium insertion and desertion reactions. It is believed that a side reactions with electrolyte could be minimized by lithium active $Co_3(PO_4)_2$ coating.

5. ACKNOWLEDGMENTS

This work was supported by Priority Research Centers Program through the National Research Foundation of Korea (NRF) funded by the Ministry of Education, Science and Technology (2009-0093818) from the World Class University (WCU) program (R33-2008-000-10003).

REFERENCES

[1] C. Delmas, I. Saadoune, A. Rougier, J. Power Sources, 44, 595 (1993).
[2] J. Cho, B. Park, J. Power Sources, 92, 35 (2001).
[3] C. Delmas, M. Ménétrier, L. Croguennec, I. Saadoune, A. Rougier, C. Pouillerie, G. Prado, M. Grüne, L. Fournès, Electrochim. Acta, 45, 243 (1999).
[4] M. Guilmard, L. Croguennec, C. Delmas, Chem. Mater., 15, 4484 (2003).
[5] S.W. Song, G.V. Zhuang, P.N. Ross, J. Electrochem. Soc., 151, A1162 (2004).
[6] K. Matsumoto, R. Kuzuo, K. Takcya, A. Yamanaka, J. Power Sources, 81, 558 (1999).
[7] H.S. Liu, Z.R. Zhang, Z.L. Gong, Y. Yang, Electrochem. Solid-State Lett., 7, A190 (2005).
[8] Y. Kim, J. Cho, J. Electrochem. Soc., 154, A495 (2007).
[9] B.V.R. Chowdari, G.V. Subba Rao, S.Y. Chow, Solid State Ionics, 140, 55 (2001).
[10] A. R. Naghash, J. Y. Lee, Electrochim. Acta, 46, 2293 (2001).
[11] S. Castro-García, A. Castro-Couceiro, M.A. Señarís-Rodríguez, F. Soulette, C. Julien, Solid State Ionics, 156, 15 (2003).
[12] H. Cao, B. Xia, N. Xu, C. Zhang, J. Alloy. Compd., 376, 282 (2004).
[13] G.V. Zhuang, G. Chen, J. Shim, X. Song, P.N. Ross, T.J. Richardson, J. Power Sources, 134, 293 (2004).
[14] H.S. Liu, Z.R. Zhang, Z.L. Gong, Y. Yang, Solid State Ionics, 166, 317 (2004).
[15] H. Lee, Y.J. Kim, Y.S. Hong, Y.J. Kim, M.G. Kim, N.S. Shin, J.P. Cho, J. Electrochem. Soc., 153, A781 (2006).
[16] K.S. Tan, M.V. Reddy, G.V. Subba Rao, B.V.R. Chowdari, J. Power Sources, 141, 129 (2005).
[17] W. Li, J.N. Reimer, J.R. Dhan, Solid State Ionics, 67, 123 (1993).